Received: 3 July 2020 | Revised: 18 December 2020 | Accepted: 26 December 2020

DOI: 10.1002/joc.6990

RESEARCH ARTICLE

International Journal of Climatology RMetS

Dominant modes of interannual variability in precipitation over the Hengduan Mountains during rainy seasons

Weichen Tao[1] | **Gang Huang**[1,2,3] | **Danhong Dong**[1] | **Pengfei Wang**[1,4] | **Ting Yu**[5] | **Hainan Gong**[4]

[1]State Key Laboratory of Numerical Modeling for Atmospheric Sciences and Geophysical Fluid Dynamics, Institute of Atmospheric Physics, Chinese Academy of Sciences, Beijing, China

[2]Laboratory for Regional Oceanography and Numerical Modeling, Qingdao National Laboratory for Marine Science and Technology, Qingdao, China

[3]University of Chinese Academy of Sciences, Beijing, China

[4]Center for Monsoon System Research, Institute of Atmospheric Physics, Chinese Academy of Sciences, Beijing, China

[5]Luoyang Electronic Equipment Test Center of China, Jiyuan, China

Correspondence
Gang Huang and Danhong Dong, State Key Laboratory of Numerical Modeling for Atmospheric Sciences and Geophysical Fluid Dynamics, Institute of Atmospheric Physics, Chinese Academy of Sciences, Beijing, 100029, China.
Email: hg@mail.iap.ac.cn (G. H.) and
Email: dongdanhong@mail.iap.ac.cn (D. D.)

Funding information
Second Tibetan Plateau Scientific Expedition and Research (STEP) program, Grant/Award Number: 2019QZKK0102; National Natural Science Foundation of China, Grant/Award Numbers: 41831175, 41705068, 91937302, 41721004; Key Deployment Project of Centre for Ocean Mega-Research of Science, Chinese Academy of Sciences, Grant/Award Number: COMS2019Q03; Heavy Rain and Drought-Flood Disasters in Plateau and Basin Key Laboratory of Sichuan Province, Grant/Award Number: SZKT201903; China Postdoctoral Science Foundation, Grant/Award Numbers: 2016LH0005, 2016M600116

Abstract

Present study investigates the dominant modes of interannual variability in precipitation over the Hengduan Mountains (HM) during rainy seasons. The leading two empirical orthogonal function (EOF) modes of HM precipitation explain 28.4 and 13.9% of the total variance, respectively. Positive EOF1 phase features enhanced precipitation anomalies over the southern HM, and a dipole structure with wet anomalies occupying large areas from the YunGui plateau to Tibetan Plateau is observed in positive EOF2 phase. Analysis of moisture budget and omega equation indicate the importance of leading EOF modes related circulation anomalies, which bring the horizontal warm advection to the HM, favouring the anomalous upward motions and precipitation increase there. For EOF1, the HM is controlled by an anomalous quasi-barotropic cyclone. This cyclone is one part of a zonally oriented barotropic wave-like pattern highly resembling the Silk Road pattern. Besides, the SST anomalies over the Indo-Pacific sector are similar to the decaying phase of La Niña, which induces the wet anomalies and further triggers the anomalous lower-level cyclone as a Rossby wave response. For EOF2, an anomalous cyclone appears over the Northeast Asia from lower to upper levels, and southerly wind anomalies prevail over the HM. The North Atlantic Oscillation and its coupled tripole SST pattern trigger a zonal wave-like pattern at middle and high latitudes emanating from the Central Europe, across Mongolia to Northeast Asia. Moreover, the SST anomalies over the Indo-Pacific sector resemble the developing phase of El Niño, which induces the meridional Pacific-Japan/East Asia-Pacific teleconnection from tropical NWP to Northeast Asia.

KEYWORDS

dominant EOF modes, ENSO, moisture budget and omega equation, North Atlantic oscillation, Pacific-Japan/East Asia-Pacific teleconnection, rainy-season precipitation, silk road pattern, the Hengduan Mountains

1 | INTRODUCTION

On the southeast side of the Tibetan Plateau (TP), mountains and rivers are alternately distributed, forming the unique three-dimensional landscape featured with high mountains and deep valleys, which block east–west traffic, so this area is called "Hengduan" Mountains (HM). Within a distance of 500 km, the HM features the world's steepest elevation drop of about 4,000 m from the TP to the Sichuan basin (Figure 1). Several major Asian rivers originate from or flow through this place, as the Yangtze River and Yellow River in China, the Mekong River and Salween River over the Indochina Peninsula, and so on. Precipitation is a key variable to the formation of glaciers, the supply of freshwater from surface runoffs, and river discharge over the HM, flourishing a global biodiversity hotspot with a vascular flora of about 12,000 species (e.g., Myers *et al*., 2000; Nie *et al*., 2002; Xing and Ree, 2017; Cheng *et al*., 2018). Therefore, precipitation anomalies there have a great impact on the hydrological cycle, ecological environment, and social economy in both local and remote downstream areas.

The HM is the transition zone between the South Asian and East Asian monsoons (Fig. 7b of Dong *et al*., 2018), which contribute to the complex and changeable climate in this area (Zhu *et al*., 2013; Zhang *et al*., 2014). Zhang *et al*. (2015) found positive correlation between HM rainfall anomalies and East Asian summer monsoon. Zhu *et al*. (2016) indicated that the unstable rainfall time of South Asian monsoon largely determines the drought in the HM. The variation in the intensity of monsoon and the timing of monsoon onset and retreat are likely to result in wet and dry anomalies over the HM (e.g., Simmonds *et al*., 1999; Wang *et al*., 2001; Zhou *et al*., 2009; Tan *et al*., 2018).

It has been generally recognized that monsoon climate is influenced not only by the variations from tropics, that is, El Niño-Southern Oscillation (ENSO; e.g., Wang *et al*., 2000; Lau and Weng, 2001; Lau and Wu, 2001; Xie *et al*., 2009; Chowdary *et al*., 2019), Indian Ocean Dipole (IOD; e.g., Guan and Yamagata, 2003; Saji and Yamagata, 2003; Yuan *et al*., 2008; Qiu *et al*., 2014), but also by the atmospheric processes at middle and high latitudes, that is, Silk Road pattern (SRP; e.g., Lau and

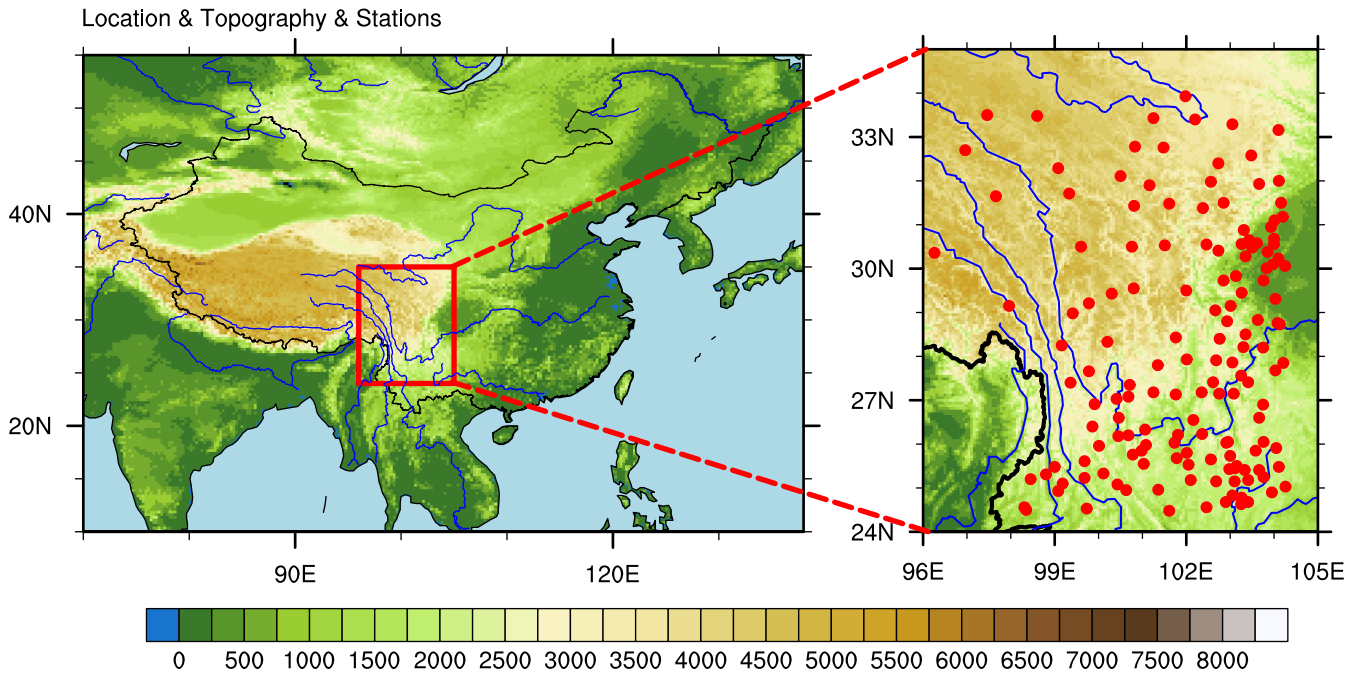

FIGURE 1 Geographic location of HM (rectangular box) and distribution of 151 stations [Colour figure can be viewed at wileyonlinelibrary.com]

Wu, 2001; Lu *et al*., 2002; Wu, 2002; Enomoto *et al*., 2003; Ding and Wang, 2005; Kosaka *et al*., 2009; Gong *et al*., 2018), North Atlantic Oscillation (NAO; e.g., Wu *et al*., 2009; Gong *et al*., 2011; Sun and Wang, 2012; Song *et al*., 2014; Chen *et al*., 2020). Recent studies have confirmed that the HM precipitation is largely controlled by the tropical sea surface temperature (SST) and mid- and high-latitude atmospheric modes at different time scales (Dong *et al*., 2018; Dong *et al*., 2019). In particular, Dong *et al*. (2018) revealed that the interannual variability of HM precipitation during rainy seasons is influenced by central and eastern Pacific (CEP) SST anomalies and SRP, and the combined effect of these two factors is briefly discussed.

Expanding the work of Dong *et al*. (2018), the aim of present study is to obtain the dominant modes of interannual variability in HM precipitation during rainy seasons, specifically distinguishes the corresponding roles of SST and atmospheric processes in each mode, and explore the possible linkage mechanism between factors from a coupled perspective. The rest of the paper is organized as follows. Section 2 describes the data and methods. Section 3 performs an empirical orthogonal function (EOF) analysis to obtain the leading two modes of HM precipitation during rainy seasons, and associated atmospheric circulation anomalies are analysed. Section 4 investigates the roles of SST and atmospheric modes in the formation of anomalous circulation, followed by a concluding summary in Section 5.

2 | DATA AND METHODS

The present study employs observed daily precipitation data from the National Climatic Center of the China Meteorological Administration (NCC/CMA) with 2,472 high density national meteorological stations. HM region is defined as a rectangular domain of 24°40′–34°00′N and 96°20′–104°30′E (Figure 1), and the stations with more than 7 consecutive days' default values are eliminated. As a result, 151 stations in HM are selected for analysis. The rainy seasons of HM are from May to September, and the total precipitation during rainy seasons accounts for more than 80% of annual total precipitation (Gao *et al*., 2013; Dong *et al*., 2018; Dong *et al*., 2019; Tao *et al*., 2020). Besides, monthly global land-surface precipitation dataset based on rain gauges from the Global Precipitation Climatology Centre Full Data Reanalysis Version 6.0 (GPCC V6; Schneider *et al*., 2014) with a spatial resolution of $0.5^\circ \times 0.5^\circ$ is used to verify its consistency with station observations. The observed topography dataset is from Earth topography one arc-minute grid (ETOPO1; Amante and Eakins, 2009) that is a 1 arc-minute global relief model of Earth's surface that integrates land topography and ocean bathymetry derived from several sources on a $1' \times 1'$ grid and is available at https://www.ngdc.noaa.gov/mgg/global/global.html.

Monthly and daily atmospheric variables used in this study are obtained from Japanese 55-year Reanalysis (JRA-55) on a $1.25^\circ \times 1.25^\circ$ horizontal resolution at 37 pressure levels, compiled by the Japan Meteorological Agency (Kobayashi *et al*., 2015; Harada *et al*., 2016). The variables include precipitation, evaporation, horizontal winds, vertical pressure velocity, specific humidity, surface pressure, air temperature, and geopotential height. According to the results of our previous studies, JRA55 well capture the climatology (Tao *et al*., 2020), interannual (Dong *et al*., 2018), and interdecadal (Dong *et al*., 2019) characteristics of HM precipitation. The monthly SST data is from NOAA Extended Reconstructed Sea Surface Temperature (ERSST) V5 on a $2^\circ \times 2^\circ$ grid (Smith and Reynolds, 2003). The study period of above data is selected from 1958 to 2017 considering the length of station observations' record and JRA-55. The monthly mean climatology is first calculated for the study period. Then, interannual anomalies are computed as the departure from the climatology. Present study focuses on the interannual variability. To extract interannual signals, we perform a 9-year running average, and only variations with periods shorter than 9 years have been retained for each variable. EOF, regression and correlation analysis are used, and the significance level is estimated based on the standard two-tailed Student's *t* test.

3 | DOMINANT MODES OF RAINY-SEASON PRECIPITATION

We perform an EOF analysis to identify the dominant modes of interannual variability in HM rainy-season mean precipitation based on 151 station observations for the period 1958–2017. Figure 2a,b shows the regression of rainy-season precipitation with respect to the leading two principal components (PCs). The first and second EOF mode (EOF1 and EOF2) explain 28.4 and 13.9% of the total variance, respectively, and these two modes are well separated according to North *et al*. (1982). Positive EOF1 phase is characterized by enhanced precipitation anomalies over the southern HM (Figure 2a), and positive EOF2 phase exhibits a dipole structure with wet anomalies occupying large areas from the YunGui plateau to TP and dry anomalies around the Sichuan basin (Figure 2b). Note that highly consistent precipitation patterns can also be seen in the regression of precipitation

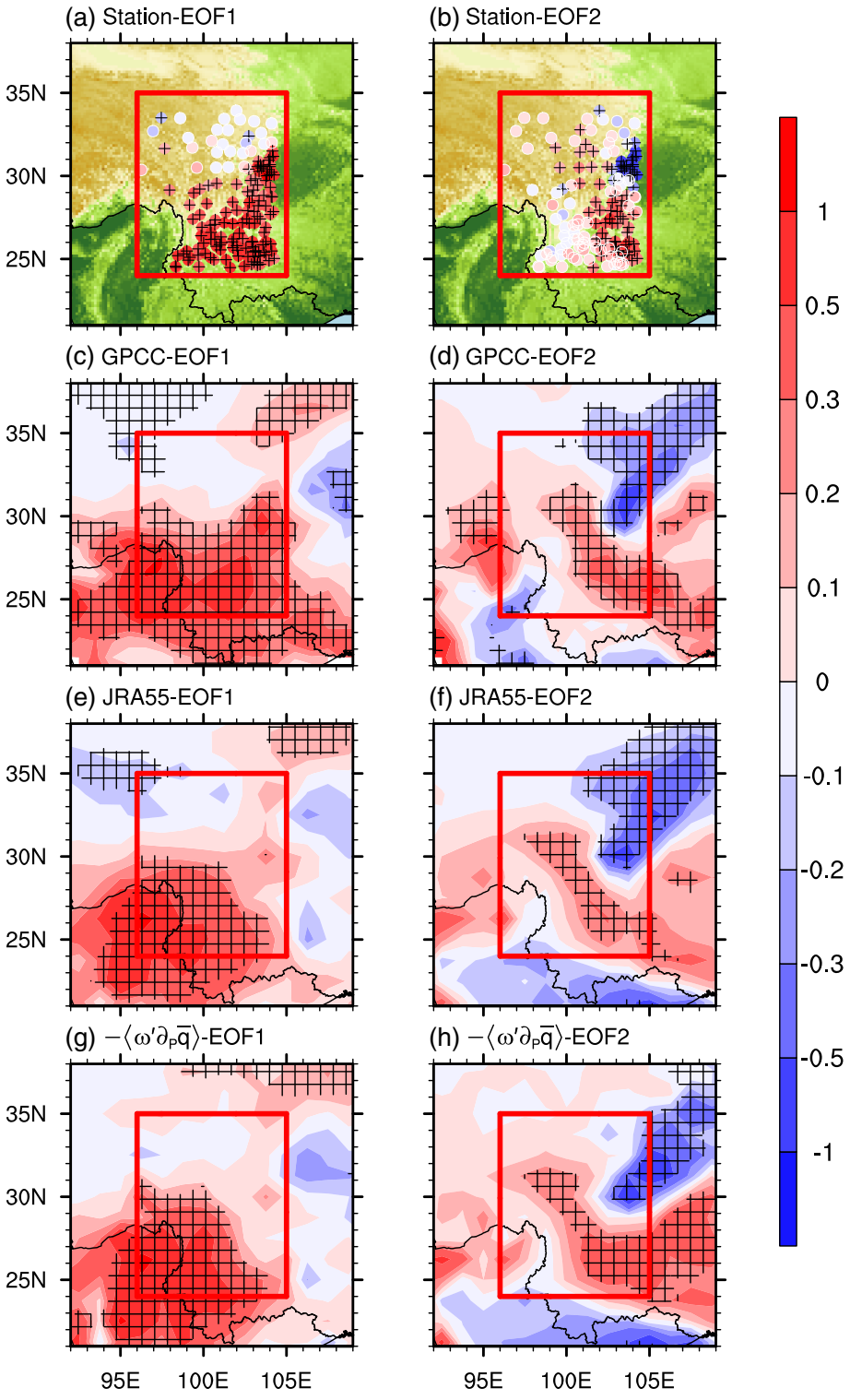

FIGURE 2 Regression of rainy-season precipitation (mm) from 151 station observations (first row, a, b), GPCC V6 (second row, c, d), and JRA-55 (third row, e, f) with respect to the normalized PC1 (left panels) and PC2 (right panels) of interannual variability in HM rainy-season precipitation based on 151 station observations for the period 1958–2017. Corresponding vertical advection of the climatological vertical moisture by anomalous vertical motions ($-\langle\omega'\partial_p\bar{q}\rangle$; mm) from budget analysis of the moisture equation based on JRA-55 (fourth row, g, h). Cross marks in (a), (b) and lattices in (c)–(h) indicate that the significance level reaches 10% [Colour figure can be viewed at wileyonlinelibrary.com]

from GPCC V6 and JRA-55 with respect to PCs obtained from 151 station observations (Figure 2c–f), documenting the reliability of using GPCC V6 and JRA-55 for further analysis in present study. Further, solution to budget analysis of the moisture equation based on JRA-55 atmospheric variables is performed to understand the mechanisms responsible for HM precipitation anomalies in the leading two modes.

3.1 | Moisture budget analysis

The anomalous precipitation can be diagnosed as

$$P' = -\langle\bar{\mathbf{V}}\cdot\nabla_h q'\rangle - \langle\mathbf{V}'\cdot\nabla_h\bar{q}\rangle - \langle\bar{\omega}\partial_p q'\rangle - \langle\omega'\partial_p\bar{q}\rangle + E'$$

where the overbars denote rainy-season climatology state; the primes denote regressed anomalies onto the

leading PCs; the angle brackets denote mass integration through an entire atmospheric column; P is the precipitation, $\mathbf{V} = (u, v)$ is the horizontal wind velocity, q is the specific humidity, ω is the vertical pressure velocity, and E is the evaporation.

According to the results of moisture budget analysis, the precipitation anomalies are dominantly contributed by the vertical advection of the climatology vertical moisture by the anomalous vertical motions ($-\langle\omega'\partial_p\bar{q}\rangle$) in the leading two EOF modes, compared with the other terms (Figure 3). Besides, the spatial patterns of precipitation anomalies highly resemble these of $-\langle\omega'\partial_p\bar{q}\rangle$ (Figure 2e–h), which emphasize the crucial role of anomalous vertical motions in the formation of precipitation anomalies.

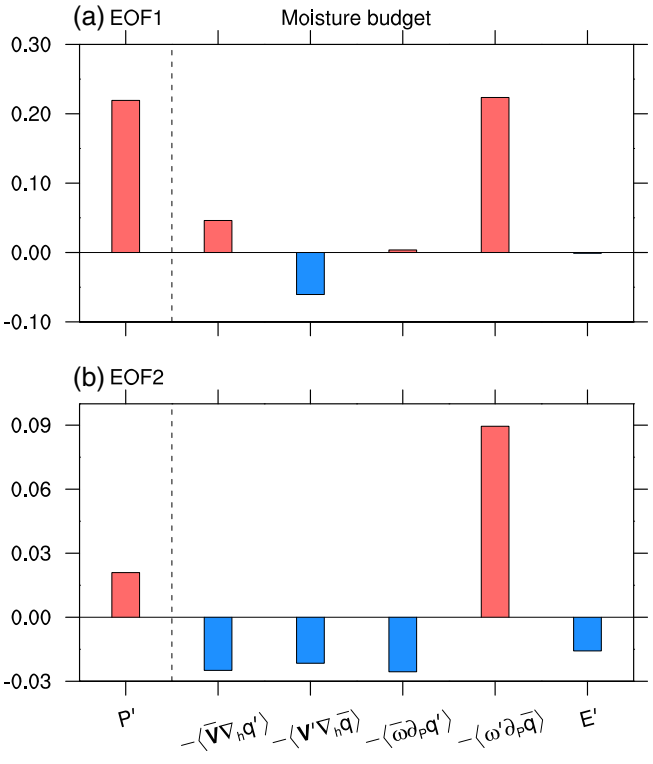

FIGURE 3 Moisture budget analysis of (a) PC1 and (b) PC2 regressed rainy-season precipitation anomalies (mm) averaged over the HM (24°40′–34°00′N, 96°20′–104°30′E) [Colour figure can be viewed at wileyonlinelibrary.com]

3.2 | Omega equation analysis

The omega equation is further used to diagnose the vertical motion anomalies over the HM at 400 and 500 hPa, where show the maximum ascending anomalies related to EOF1 and EOF2 of HM rainy-season precipitation, respectively (Figure 4; Kosaka and Nakamura, 2010; Wei *et al.*, 2014; Zhao *et al.*, 2015; Hu *et al.*, 2017; Dong *et al.*, 2018):

$$\omega' = \left(\nabla^2 + \frac{f^2}{\sigma^2}\frac{\partial^2}{\partial P^2}\right)^{-1}\frac{f}{\sigma}\frac{\partial}{\partial P}[\bar{\mathbf{V}}\cdot\nabla\zeta' + \mathbf{V}'\cdot\nabla(f+\bar{\zeta})] + \left(\nabla^2 + \frac{f^2}{\sigma^2}\frac{\partial^2}{\partial P^2}\right)^{-1}\frac{R}{\sigma P}\nabla^2(\bar{\mathbf{V}}\cdot\nabla T' + \mathbf{V}'\cdot\nabla\bar{T}) - \left(\nabla^2 + \frac{f^2}{\sigma^2}\frac{\partial^2}{\partial P^2}\right)^{-1}\frac{R}{\sigma P c_p}\nabla^2 Q$$

where $\sigma = \frac{R}{P}\left(\frac{R\bar{T}}{c_p P} - \frac{d\bar{T}}{dP}\right)$ is static stability,, f is Coriolis parameter, P is air pressure, ζ is relative vorticity, R is gas constant, T is air temperature, c_p is specific heat at constant pressure, Q is diabatic heating. The terms on the right side of the equation denote the anomalous vertical motions due to vertical difference of vorticity horizontal advection (ω'_{vor}), horizontal temperature advection (ω'_{therm}), and diabatic heating (ω'_Q), respectively. Figures 5 and 6 show the diagnosed results of omega equation in regional average and spatial distribution, respectively. Except for ω_Q that is considered as a circulation-precipitation feedback (Hu *et al.*, 2017; Tao *et al.*, 2020), ω'_{therm} contributes more to the ascending anomalies than ω'_{vor} for both two EOF modes (Figures 5 and 6a–d).

Further decomposition of ω'_{therm} shows that the anomalous temperature advected by the climatology horizontal winds ($\bar{\mathbf{V}}\cdot\nabla T'$) and the climatology temperature advected by the anomalous horizontal winds ($\mathbf{V}'\cdot\nabla\bar{T}$) are equally important in EOF1 (Figures 5a, 6c,e,g), and $\mathbf{V}'\cdot\nabla\bar{T}$ is stronger than $\bar{\mathbf{V}}\cdot\nabla T'$ in EOF2 (Figures 5b, 6d,f, h). During rainy seasons, climatology westerlies prevail in the midtroposphere and transport PCs related warm temperature anomalies to the HM (Figure 6e,f). Moreover, climatology air temperature over the TP is higher than the surrounding regions, and the two EOF modes related circulation anomalies bring warm air to the HM (Figure 6g,h). As a result, the intensified warm advection induces the anomalous midtropospheric upward motions, which further lead to the precipitation anomalies in the leading two EOF modes. Note that the climatology circulation and temperature generally reflect the effect of unique topography and location of HM. Besides, the anomalous temperature and winds around the HM are well coupled, and the anticyclonic wind anomalies

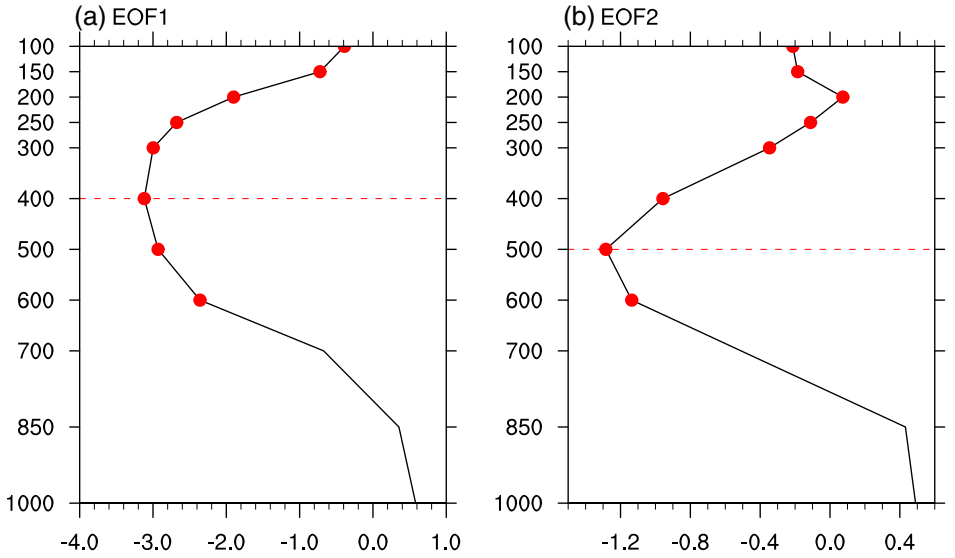

FIGURE 4 Vertical profile of (a) PC1 and (b) PC2 regressed rainy-season vertical pressure velocity anomalies (10^{-3} Pa·s^{-1}) averaged over the HM (24°40′–34°00′N, 96°20′–104°30′E). Dots indicate that the significance level reaches 10% [Colour figure can be viewed at wileyonlinelibrary.com]

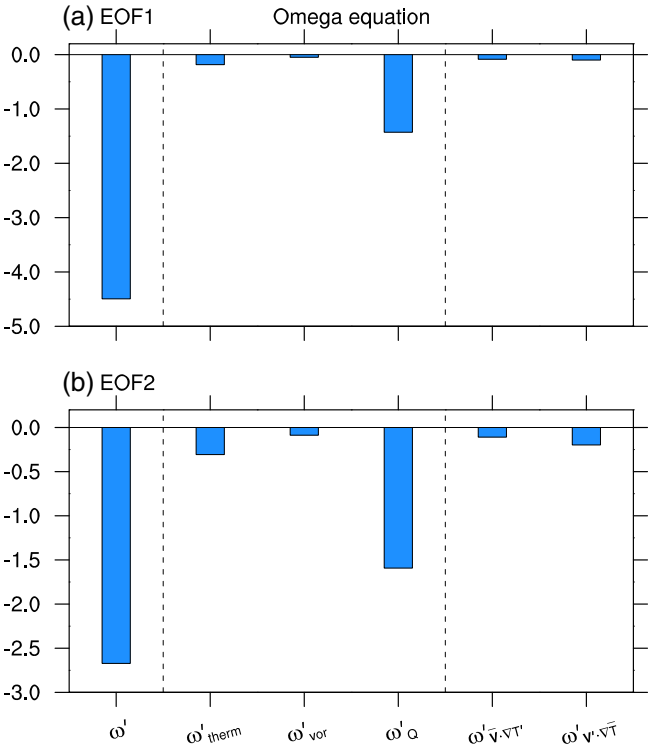

FIGURE 5 Omega equation analysis of (a) PC1 and (b) PC2 regressed rainy-season vertical pressure velocity (10^{-3} Pa·s^{-1}) anomalies from JRA-55 over the HM (24°40′–34°00′N, 96°20′–104°30′E) [Colour figure can be viewed at wileyonlinelibrary.com]

accompany with the warm anomalies, and vice versa (Figure 6e–h), indicating the importance of circulation anomalies.

Figure 7 illustrates the regression of rainy-season geopotential height and horizontal winds at 200, 500, and 850 hPa with respect to the normalized PC1 and PC2. Corresponding to EOF1 of rainy-season HM precipitation, the HM is controlled by an anomalous middle- and lower- level cyclone over the southern China (Figures 6g, 7a,c), and the anomalous cyclone with negative geopotential height anomalies slightly shifts northwestward to Central China at upper levels (Figure 7e), displaying a quasi-barotropic structure. While for EOF2, southerly wind anomalies from lower to upper levels prevail over the HM, where is at the southwest side of the anomalous cyclone over the Northeast Asia (Figures 6h, 7b,d,f). The possible factors contributing to the circulation anomalies around the HM related to the leading two EOF modes, as well as the underlying processes, will be investigated in the next section.

4 | ROLES OF SST AND ATMOSPHERIC MODES

4.1 | EOF1

Corresponding to EOF1, the anomalous cyclone around the HM accompanied by the negative geopotential height anomalies is one part of a zonally oriented barotropic wave-like pattern, which is trapped along the subtropical Asian jet stream, with anomalous positive geopotential height centres over the North Atlantic Ocean, West Asia, and Northeast Asia, and anomalous negative geopotential height centres over the Central Europe and Central China (Figure 7a,c,e). The whole structure highly resembles the SRP (Figure S1a), with a pattern correlation coefficient at 0.74 for geopotential height over 20°–80°N, 0°–150°E. The SRP index is defined as the PC1 of 200 hPa meridional winds over 20°–80°N, 30°W–150°E during rainy seasons. The correlation coefficient between PC1 of HM precipitation and SRP index is 0.36, exceeding the

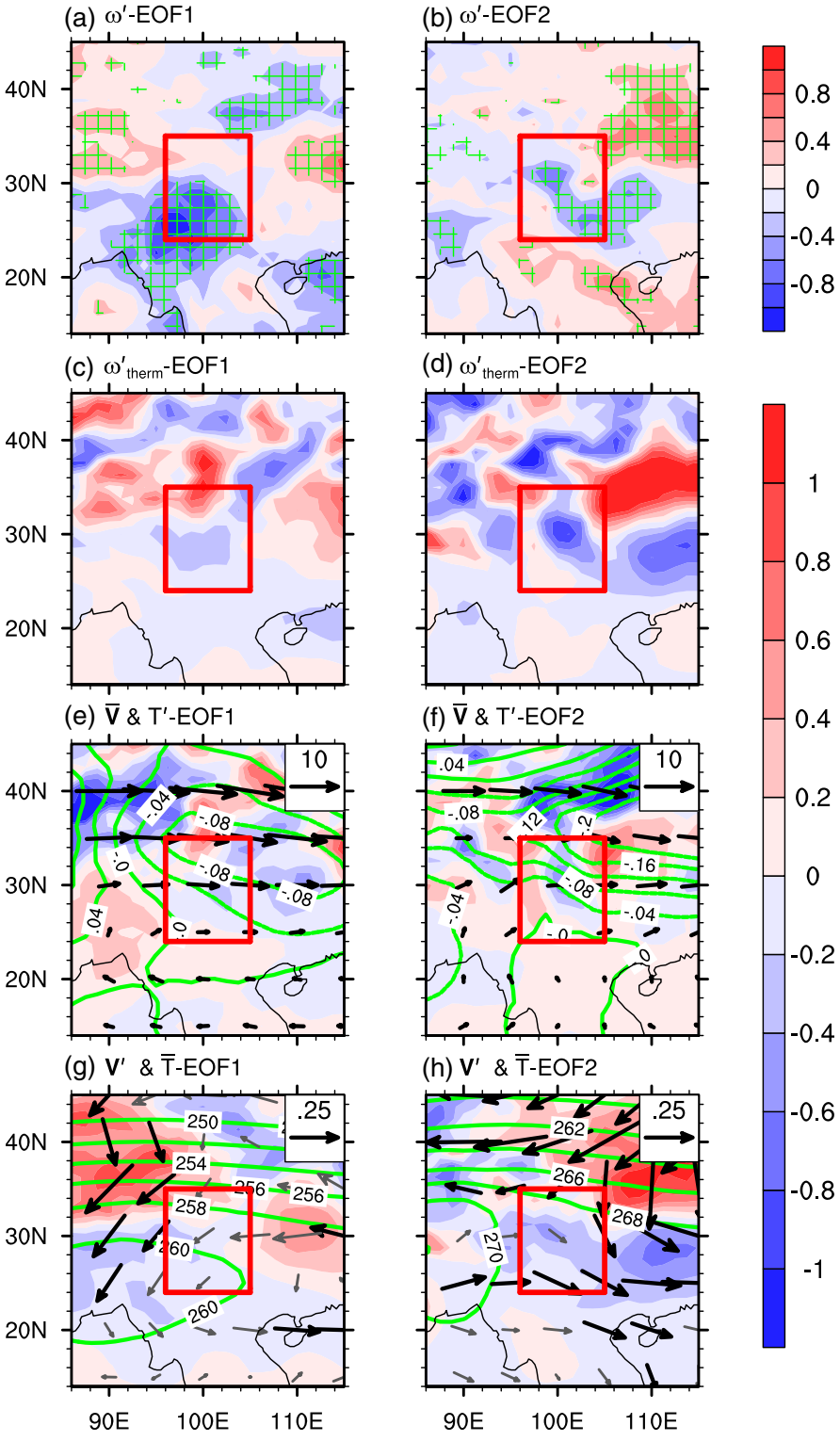

FIGURE 6 Regression of rainy-season 400 and 500 hPa vertical pressure velocity (10^{-3} Pa·s^{-1}) based on JRA-55 with respect to the normalized (a) PC1 and (b) PC2, respectively. Corresponding horizontal temperature advection (ω'_{therm}; 10^{-3} Pa·s^{-1}), the advection (shaded; 10^{-3} Pa·s^{-1}) of anomalous temperature (contour; K) advected by climatology horizontal winds (vectors; m·s^{-1}), and the advection (shaded; 10^{-3} Pa·s^{-1}) of climatology temperature (contour; K) advected by anomalous horizontal winds (vectors; m·s^{-1}) from budget analysis of the omega equation based on JRA-55 for EOF1 (left panels; c, e, g) and EOF2 (right panels; d, f, h). Lattices in (a), (b) and black vectors in (g), (h) indicate that the significance level reaches 10% [Colour figure can be viewed at wileyonlinelibrary.com]

1% significance level. Note that the anomalous upper-level positive geopotential height cell to the northwestern India, which has a tilted baroclinic structure with lower-level negative geopotential height anomalies over the Indian subcontinent. This baroclinic structure is induced due to the anomalous south Asian summer monsoon rainfall released heat (Wu, 2002; Ding and Wang, 2005, 2007).

In the tropics, anomalous easterlies (westerlies) at lower (upper) levels can be seen over the western Pacific (WP), associated with the positive SST anomalies in the WP and negative SST anomalies in the CEP (Figure 8a). Moreover, a significant cooling is observed in the Indian Ocean (IO). The EOF1 related SST anomalies over the Indo-Pacific exhibit a typical pattern of slow-decay

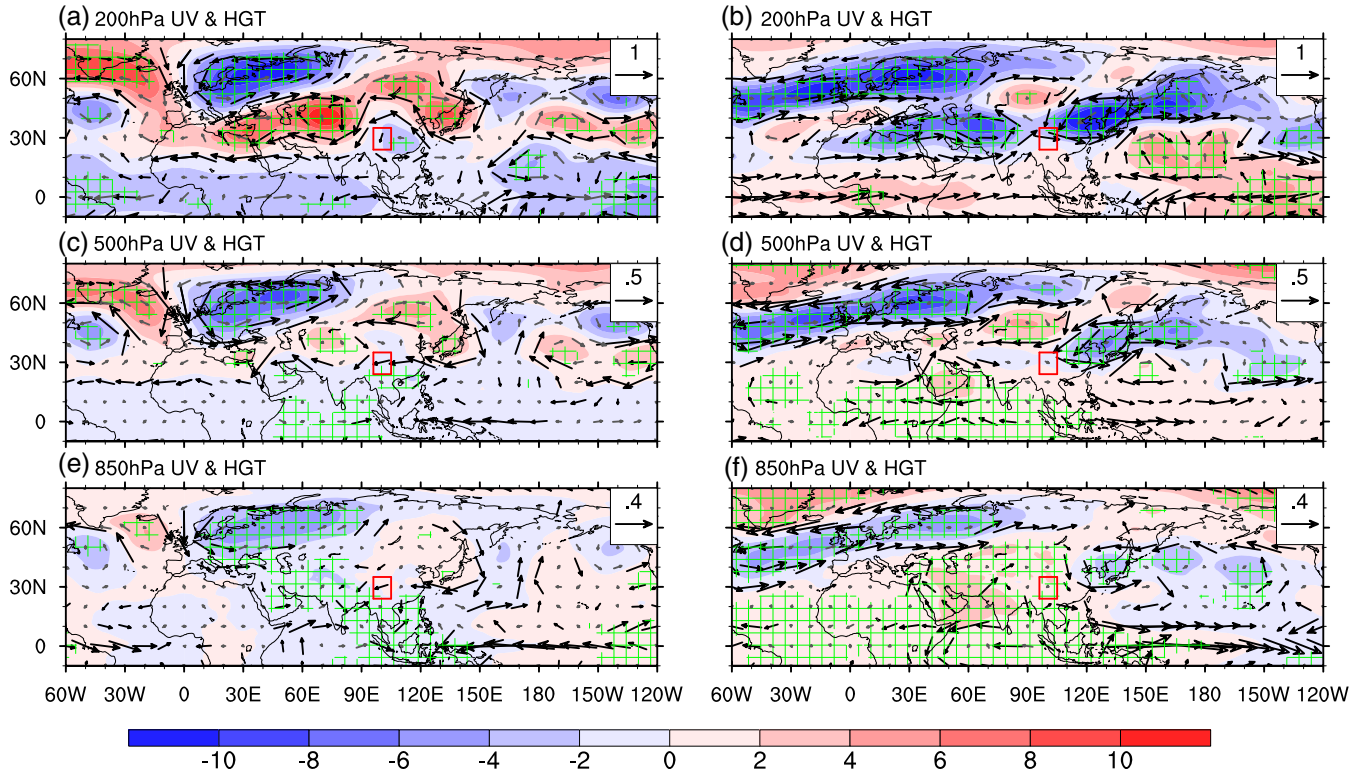

FIGURE 7 Regression of rainy-season geopotential height (shaded; gpm) and horizontal winds (vectors; $m \cdot s^{-1}$) at 200, 500, and 850 hPa based on JRA-55 with respect to the normalized PC1 (left panels; a, c, e) and PC2 (right panels; b, d, f). Lattices and black vectors indicate that the significance level reaches 10% [Colour figure can be viewed at wileyonlinelibrary.com]

ENSO, which is common for La Niña events (Chen *et al*., 2017; Li *et al*., 2017; Tao *et al*., 2017). The CEP (IO) cooling causes dry anomalies over the WP (West IO), and triggers the lower-level anticyclonic (westerly) wind anomalies over the Northwest Pacific (East IO) as a Rossby (Kelvin) wave response (Figures 7e, 8c,e), leading to the convergence and ascending anomalies over the Northwest Pacific (NWP; Chen *et al*., 2017; Tao *et al*., 2017; Dong *et al*., 2018; Tao *et al*., 2018; Tao *et al*., 2019). The resultant wet anomalies there induce the anomalous lower-level cyclone over the southern China through a Rossby wave response. Besides, the NWP warming could contribute to the anomalous cyclone as a local forcing (Wang *et al*., 2000; Wu *et al*., 2010; Wang *et al*., 2013; Wu *et al*., 2017). The PC1 of HM precipitation is correlated with SST anomalies over the CEP (5°S–5°N, 150°–90°W), IO (10°S–20°N, 40°–100°E), NWP (10°–20°N, 130°–160°E), and the whole Indo-Pacific sector (CEP+IO-NWP) during rainy seasons at −0.39, −0.33, 0.28, and −0.43, which reach 1%, 1%, 5%, and 1% significant level, respectively. The SST anomalies over the IO and NWP can be largely explained by the ENSO related atmospheric and oceanic processes (e.g., Klein *et al*., 1999; Wang *et al*., 2000; Xie *et al*., 2002; Du *et al*., 2009; Tao *et al*., 2016), indicating the crucial role of ENSO in HM precipitation.

The correlation coefficient between SRP index and CEP SST anomalies is −0.30, exceeding the 5% significance level. Thus, these two factors co-change with the EOF1 of HM precipitation supported by the significant correlation coefficients among the three of them, suggesting the combined effect of SRP and ENSO. This result is generally consistent with Dong *et al*. (2018), who firstly found that the selected abnormal years are almost concurrent based on the indexes of HM precipitation, CEP SST anomalies, and SRP. Tropical forcing is important to SRP (Lu *et al*., 2002; Ding and Wang, 2005; Yasui and Watanabe, 2010; Chen and Huang, 2012; Hong and Lu, 2016), and ENSO does not seem to affect SRP directly. Ding and Wang (2005) emphasized that ENSO exerts an influence on the SRP through the South Asian summer monsoon. On one hand, the negative SST anomalies over the CEP cools the tropospheric temperature in the tropics, increases the temperature difference between the Indian and IO, strengthens the southwesterly winds over the West IO (Figure 7e), and further enhances convection over the northwestern Indian (Figure 8c,e), where the precipitation anomalies play an active role in connecting (exciting) the upstream (downstream) SRP (Ding and Wang, 2007). On the other hand, the negative tropical tropospheric temperature anomalies cause the

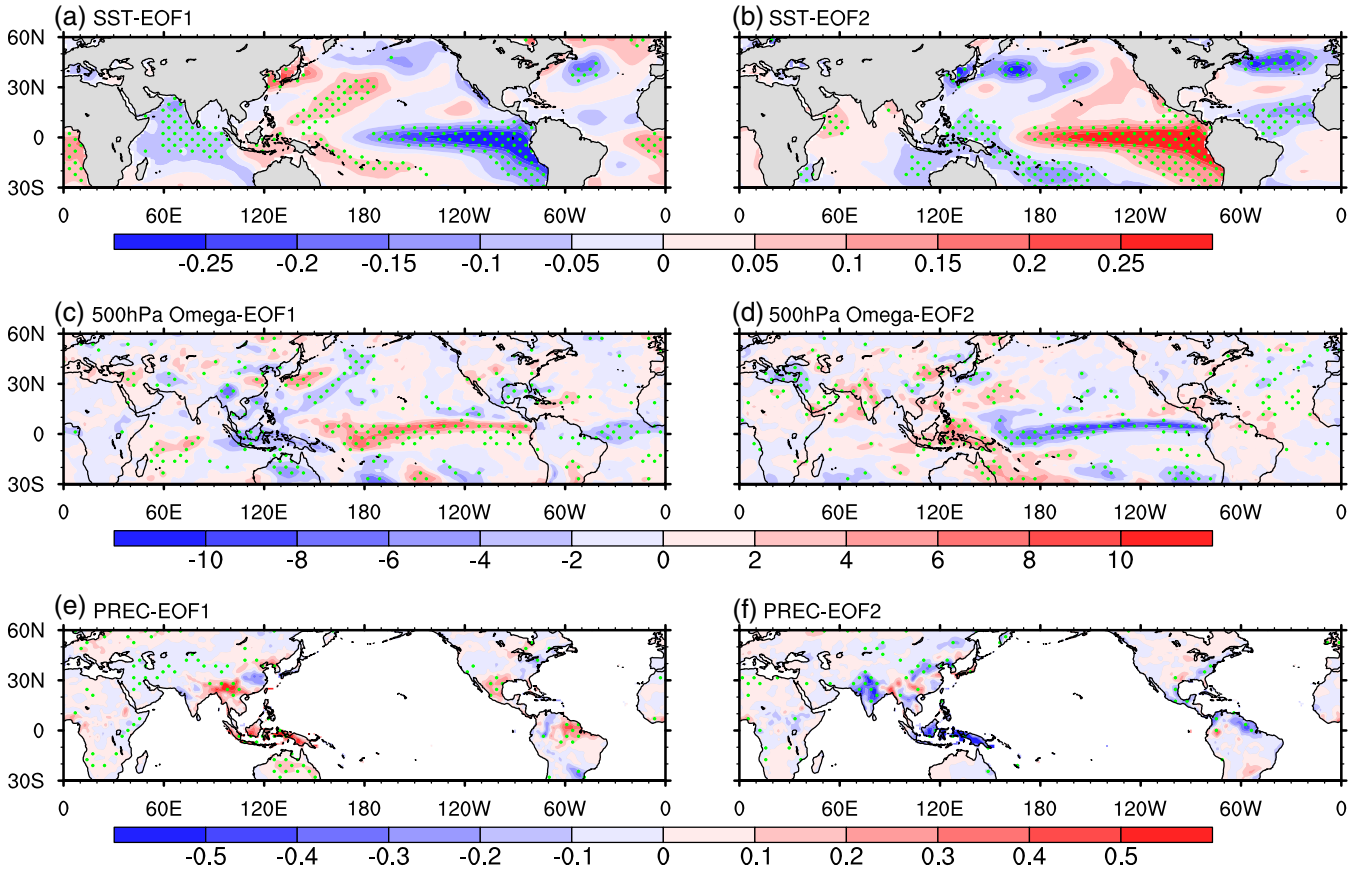

FIGURE 8 Regression of rainy-season SST (shaded; K) based on ERSST V5 with respect to the normalized (a) PC1 and (b) PC2. (c), (e) and (d), (f) are as (a) and (b), but for 500 hPa vertical pressure velocity (contour; 10^{-3} Pa·s^{-1}) based on JRA-55 and precipitation (shaded; mm) based on GPCC V6, respectively. Dots indicate that the significance levels reach 10% [Colour figure can be viewed at wileyonlinelibrary.com]

northward gradient, leading to the northward displacement of the Asian jet associated with southerly wind anomalies around the eastern Mediterranean Sea (Figure 7a). Those meridional wind anomalies is located in the entrance of the Asian jet and trigger the SRP as an internal atmospheric mechanism (Hong and Lu, 2016).

4.2 | EOF2

Corresponding to EOF2 of rainy-season HM precipitation, the circulation anomalies at middle and high latitudes display a barotropic wave-like structure emanating from the Central Europe, across Mongolia to Northeast Asia (Figure 7b,d,f). Additionally, a meridional dipole structure of circulation anomalies appears over the North Atlantic Ocean, where is accompanied by a meridional tripole SST pattern (Figure 8b), analogous to positive phase of NAO (Walker, 1924; Loon and Rogers, 1978; Wallace and Gutzler, 1981). The regression of rainy-season geopotential height and horizontal winds at 200 hPa with respect to the NAO index highly resemble the EOF2 related circulation anomalies, with a pattern correlation coefficient at 0.69 over 20°–80°N, 30°W–150°E (Figure S1b). The NAO index is defined as the PC1 of sea level pressure over 25°–70°N, 70°W–50°E during rainy seasons following Folland *et al.* (2009). Previous studies have revealed that NAO and its coupled tripole SST pattern can trigger a wave pattern to affect the climate around the East Asia (e.g., Wu *et al.*, 2009; Wu *et al.*, 2011; Sun and Wang, 2012; Chen *et al.*, 2016; Wang *et al.*, 2018; Chen *et al.*, 2020). The indices used to represent the meridional tripole SST (MTS) anomalies over the North Atlantic Ocean and zonal tripole pattern (ZTP) over the Eurasia are constructed as the sum of two regions with negative values minus the region with positive values for SST anomalies and 200 hPa geopotential height anomalies in Figures 8b and 7b, respectively (Table 1). The PC2, NAO index, MTS index, and ZTP index are highly correlated with each other and reach 1% significance level (Table 1), supporting the idea of NAO and its coupled tripole SST pattern induced wave-like pattern affecting HM precipitation.

TABLE 1 Correlation coefficients among PC2, NAO, MTS, and ZTP indices

	PC2	NAO	MTS	ZTP
PC2	/	0.37**	−0.39**	−0.62**
NAO	/	/	−0.37**	−0.45**
MTS	/	/	/	0.44**
ZTP	/	/	/	/

Note: Correlation coefficients with two asterisks indicate that the significance level reaches 1%. The NAO index is defined as the PC1 of sea level pressure over 25°–70°N, 70°W–50°E during rainy seasons following Folland *et al.* (2009). The MTS index is constructed as the sum of two regions with negative values over 5°–20°N, 50°–20°W, and 35°–50°N, 60°–30°W minus the region with positive values over 20°–30°N, 50°–30°W for SST anomalies in Figure 8b. The ZTP index is constructed as the sum of two regions with negative values over 55°–65°N, 20°–40°E, and 35°–45°N, 120°–130°E minus the region with positive values over 45°–55°N, 85°–95°E for 200 hPa geopotential height anomalies in Figure 7b.

TABLE 2 Correlation coefficients between PC2, EAP and EAP, Niño3, IOD, and the whole indo-Pacific (Niño3+IOD) indices

	EAP	Niño3	IOD	Niño3+IOD
PC2	−0.47**	0.48**	0.39**	0.51**
EAP	/	−0.32*	−0.23	−0.32*

Note: Correlation coefficients with one and two asterisks indicate that the significance level reaches 5 and 1%, respectively. The EAP index is constructed as the grid point at 40°N, 125°E minus the two grid points at 60°N, 125°E and 20°N, 125°E for 500 hPa geopotential height anomalies in Figure 7d, following Huang (2004). The Niño3 index is defined as SST anomalies averaged over 5°S–5°N, 150°–90°W. The IOD index is constructed as the difference of SST anomalies averaged over 0°–20°N, 40°–70°E, and 30°–10°S, 90°–120°E.

Besides, a meridional tripole pattern of circulation anomalies at middle and lower levels is observed from tropical NWP to Northeast Asia and generally recognized as the Pacific-Japan/East Asia-Pacific (PJ/EAP) teleconnection (Nitta, 1987; Huang and Sun, 1992). Anomalous lower- (upper-) level divergence (convergence) is obviously observed over the tropical WP (Figure 7b,f), suppressing the convection there (Figure 8d,f). The corresponding SST pattern over the Indo-Pacific sector exhibits a zonal tripole structure with positive IOD-like and El Niño-like SST anomalies resembling the developing phase of El Niño (Figure 8b) (Annamalai *et al.*, 2005; Li *et al.*, 2015ab), which suppress the WP convection through zonal circulation adjustment. The PJ/EAP teleconnection is triggered due to the propagation of quasi-stationary planetary waves forced by the source around the WP with the dry anomalies (Nitta, 1987; Huang and Sun, 1992). The PC2 of HM precipitation is significantly correlated with EAP index, Niño3 index, IOD index, and the SST anomalies over the whole Indo-Pacific sector (Niño3+IOD) at −0.47, 0.48, 0.39, and 0.51, respectively (Table 2). Furthermore, the PJ/EAP teleconnection is dominantly controlled by CEP SST anomalies (Table 2), and the Niño3 regressed circulation anomalies highly resemble the PC2 related circulation anomalies from lower to upper levels and capture the PJ/EAP pattern over the NWP (Figure S2a–c). Thus, these results document that ENSO could influence HM precipitation through the PJ/EAP teleconnection. It is noteworthy that, beside ENSO forced variability, the PJ/EAP teleconnection is also largely influenced by atmospheric internal variability (Kosaka and Nakamura, 2011), as well as the non-ENSO forced air-sea coupled variability (Kosaka *et al.*, 2013).

Ham *et al.* (2013) revealed that the SST anomalies in the north tropical Atlantic during boreal spring can serve as a trigger for ENSO events. The north tropical Atlantic SST anomalies are one part of the anomalous tripole SST pattern, which is usually coupled with NAO (e.g., Wu *et al.*, 2009; Wu *et al.*, 2011; Sun and Wang, 2012; Chen *et al.*, 2016; Wang *et al.*, 2018; Chen *et al.*, 2020). Thus, these conclusions suggest that NAO could trigger ENSO events via north tropical Atlantic SST anomalies. However, in present study, the relationship between NAO and developing El Niño is not clear as the insignificant correlation coefficient between them. One possible reason is that the developing El Niño is an indirect response to NAO. The north tropical Atlantic SST has strong interannual variability contributed by multiple factors (Wu and Liu, 2002; Xie and Carton, 2004; Chang *et al.*, 2006), and NAO is only one factor of them.

5 | CONCLUSION AND DISCUSSION

The present study investigates the dominant modes of interannual variability in precipitation over the HM during rainy seasons based on various observational and reanalysis datasets. The leading two EOF modes of HM precipitation explain 28.4 and 13.9% of the total variance, respectively. Positive EOF1 phase features enhanced precipitation anomalies over the southern HM, and a dipole structure with wet anomalies occupying large areas from the YunGui plateau to TP and dry anomalies around the Sichuan basin is observed in positive EOF2 phase.

According to the results of moisture budget analysis, the precipitation anomalies in the leading two modes are largely contributed by $-\langle \omega' \partial_p \bar{q} \rangle$, which emphasize the crucial role of anomalous vertical motions. Analysis of omega equation indicates that the dominant role of horizontal warm advection in anomalous upward motions over the HM, and further decomposition of horizontal

temperature advection finds that $\bar{\mathbf{V}} \cdot \nabla T'$ and $\mathbf{V}' \cdot \nabla \bar{T}$ are important in the leading two EOF modes. Climatology westerlies prevail over the HM, and climatology air temperature over the TP is higher than the surrounding regions. Together with the leading two EOF modes related temperature and circulation anomalies, the warm advection is generated over the HM, favouring the anomalous upward motions there. Since the temperature anomalies are coherent with circulation anomalies, the horizontal warm advection reflects the importance of anomalous circulation, which controls the leading modes of HM precipitation.

Corresponding to EOF1 of HM precipitation, the HM is controlled by an anomalous middle- and lower-level cyclone over the southern China, and the anomalous cyclone slightly shifts northwestward to Central China at upper levels, displaying a quasi-barotropic structure. On one hand, the anomalous cyclone around the HM is one part of a zonally oriented barotropic wave-like pattern trapped along the subtropical Asian jet stream from the North Atlantic Ocean to Northeast Asia, highly resembling the SRP. On the other hand, the SST anomalies over the Indo-Pacific sector are similar to the decaying phase of La Niña. The CEP and IO cooling and the NWP warming contribute to the lower-level convergence and wet anomalies over the NWP, triggering the anomalous lower-level cyclone over the southern China as a Rossby wave response. Moreover, the SRP has a close relationship with the CEP SST anomalies, indicating their combined effect to the HM precipitation.

Corresponding to EOF2 of HM precipitation, an anomalous cyclone appears over the Northeast Asia from lower to upper levels, and southerly wind anomalies at its southwest side prevail over the HM. The NAO and its coupled tripole SST pattern trigger a zonal wave-like pattern at middle and high latitudes emanating from the Central Europe, across Mongolia to Northeast Asia. Besides, the SST anomalies over the Indo-Pacific sector resemble the developing phase of El Niño, which induces the meridional PJ/EAP teleconnection from tropical NWP to Northeast Asia.

Interestingly, the positive EOF1 and EOF2 phase show the enhanced precipitation anomalies over the HM, and correspond with the opposite ENSO phase, respectively. That is to say, both El Niño and La Niña favour the increase of HM precipitation. It seems contradictory, but ENSO varies greatly form one event to another for spatial pattern (Ashok *et al*., 2007; Kao and Yu, 2009; Kug *et al*., 2009; Yeh *et al*., 2009; Tao *et al*., 2014), amplitude (Su *et al*., 2010; Takahashi and Dewitte, 2016; Wang *et al*., 2019), and temporal evolution (Trenberth and Stepaniak, 2001; Ohba and Ueda, 2007; Okumura and Deser, 2010; Hu *et al*., 2013; Lee *et al*., 2014). Thus, ENSO diversity cause that its atmospheric teleconnections and impacts are different. There are some discrepancies between the two EOF modes related SST anomalies over the Indo-Pacific sector. In the Pacific, the CEP warming corresponding to EOF2 is stronger and extends more westward than the CEP cooling corresponding to EOF1 (Figure 9a,b). In the IO, a basin-wide cooling and a zonal dipole SST pattern are observed for EOF1 and EOF2, respectively. As a result, an anomalous lower-level cyclone over the southern China is induced in EOF1, while the PJ/EAP teleconnection is triggered in EOF2.

The present study focuses on the HM precipitation during the whole rainy seasons, which start from May to September. However, the SST and atmospheric modes and their contribution to the leading EOF modes of HM precipitation for each month of rainy seasons are likely to be different. For instance, Yang *et al*. (2020) investigates the impacts of tropical Indo-Pacific SST anomalies on interannual precipitation variations over the Indochina Peninsula during the rainy seasons, and more precipitation in May–June, July–August, and October–November occurs in the La Niña decaying years, La Niña decaying years and/or El Niño developing years, and La Niña developing years, respectively. Thus, the month-to-month discrepancies of SST and atmospheric modes affecting interannual variability of HM precipitation during rainy seasons are deserved to be further investigated in the future.

ACKNOWLEDGEMENTS

This work was supported by the Second Tibetan Plateau Scientific Expedition and Research (STEP) program (2019QZKK0102), the National Natural Science Foundation of China (41831175, 41705068, 91937302, and 41721004), the Key Deployment Project of Centre for Ocean Mega-Research of Science, Chinese Academy of Sciences (COMS2019Q03), the Heavy Rain and Drought-Flood Disasters in Plateau and Basin Key Laboratory of Sichuan Province (SZKT201903), and the China Postdoctoral Science Foundation (2016LH0005 and 2016M600116).

ORCID

Weichen Tao https://orcid.org/0000-0002-4629-576X
Gang Huang https://orcid.org/0000-0002-8692-7856

REFERENCES

Amante, C. and Eakins, B.W. (2009) ETOPO1 1 arc-minute global relief model: procedures, data sources and analysis. In: *NOAA Technical Memorandum NESDIS NGDC-24*. NOAA: National Geophysical Data Center. 10.7289/V5D798BF.

Annamalai, H., Xie, S.P., McCreary, J.P. and Murtugudde, R. (2005) Impact of Indian Ocean Sea surface temperature on developing

El Niño. *Journal of Climate*, 18(2), 302–319. https://doi.org/10.1175/jcli-3268.1.

Ashok, K., Behera, S.K., Rao, S.A., Weng, H. and Yamagata, T. (2007) El Niño Modoki and its possible teleconnection. *Journal of Geophysical Research*, 112(C11), C11007.

Chang, P., Fang, Y., Saravanan, R., Ji, L. and Seidel, H. (2006) The cause of the fragile relationship between the Pacific El Nino and the Atlantic Nino. *Nature*, 443(7109), 324–328.

Chen, G. and Huang, R. (2012) Excitation mechanisms of the teleconnection patterns affecting the July precipitation in Northwest China. *Journal of Climate*, 25(22), 7834–7851. https://doi.org/10.1175/jcli-d-11-00684.1.

Chen, S., Wu, R. and Liu, Y. (2016) Dominant modes of interannual variability in Eurasian surface air temperature during boreal spring. *Journal of Climate*, 29(3), 1109–1125. https://doi.org/10.1175/jcli-d-15-0524.1.

Chen, Z., Wen, Z., Wu, R. and Du, Y. (2017) Roles of tropical SST anomalies in modulating the western North Pacific anomalous cyclone during strong La Niña decaying years. *Climate Dynamics*, 49(1), 633–647. https://doi.org/10.1007/s00382-016-3364-4.

Chen, S., Wu, R., Chen, W., Hu, K. and Yu, B. (2020) Structure and dynamics of a springtime atmospheric wave train over the North Atlantic and Eurasia. *Climate Dynamics*, 54(11), 5111–5126. https://doi.org/10.1007/s00382-020-05274-7.

Cheng, Z., Weng, C., Guo, J., Dai, L. and Zhou, Z. (2018) Vegetation responses to late quaternary climate change in a biodiversity hotspot, the three parallel Rivers region in southwestern China. *Palaeogeography, Palaeoclimatology, Palaeoecology*, 491, 10–20. https://doi.org/10.1016/j.palaeo.2017.11.032.

Chowdary, J.S., Patekar, D., Srinivas, G., Gnanaseelan, C. and Parekh, A. (2019) Impact of the indo-Western Pacific Ocean capacitor mode on south Asian summer monsoon rainfall. *Climate Dynamics*, 53(3), 2327–2338. https://doi.org/10.1007/s00382-019-04850-w.

Ding, Q. and Wang, B. (2005) Circumglobal teleconnection in the northern hemisphere summer. *Journal of Climate*, 18(17), 3483–3505. https://doi.org/10.1175/jcli3473.1.

Ding, Q. and Wang, B. (2007) Intraseasonal teleconnection between the summer Eurasian wave train and the Indian monsoon. *Journal of Climate*, 20(15), 3751–3767. https://doi.org/10.1175/jcli4221.1.

Dong, D., Huang, G., Tao, W., Wu, R., Hu, K. and Li, C. (2018) Interannual variation of precipitation over the Hengduan Mountains during rainy season. *International Journal of Climatology*, 38(4), 2112–2125. https://doi.org/10.1002/joc.5321.

Dong, D., Tao, W., Lau, W.K.M., Li, Z., Huang, G. and Wang, P. (2019) Interdecadal variation of precipitation over the Hengduan Mountains during rainy seasons. *Journal of Climate*, 32(12), 3743–3760. https://doi.org/10.1175/jcli-d-18-0670.1.

Du, Y., Xie, S.P., Huang, G. and Hu, K. (2009) Role of Air-Sea interaction in the long persistence of El Niño-induced North Indian Ocean warming. *Journal of Climate*, 22(8), 2023–2038.

Enomoto, T., Hoskins, B.J. and Matsuda, Y. (2003) The formation mechanism of the Bonin high in august. *Quarterly Journal of the Royal Meteorological Society*, 129(587), 157–178. https://doi.org/10.1256/qj.01.211.

Folland, C.K., Knight, J., Linderholm, H.W., Fereday, D., Ineson, S. and Hurrell, J.W. (2009) The summer North Atlantic oscillation: past, present, and future. *Journal of Climate*, 22(5), 1082–1103. https://doi.org/10.1175/2008jcli2459.1.

Gao, Y., Wang, H. and Li, S. (2013) Influences of the Atlantic Ocean on the summer precipitation of the southeastern Tibetan plateau. *Journal of Geophysical Research: Atmospheres*, 118(9), 3534–3544. https://doi.org/10.1002/jgrd.50290.

Gong, D.-Y., Yang, J., Kim, S.-J., Gao, Y., Guo, D., Zhou, T. and Hu, M. (2011) Spring Arctic oscillation-east Asian summer monsoon connection through circulation changes over the western North Pacific. *Climate Dynamics*, 37(11–12), 2199–2216. https://doi.org/10.1007/s00382-011-1041-1.

Gong, Z., Feng, G., Dogar, M.M. and Huang, G. (2018) The possible physical mechanism for the EAP–SR co-action. *Climate Dynamics*, 51(4), 1499–1516. https://doi.org/10.1007/s00382-017-3967-4.

Guan, Z. and Yamagata, T. (2003) The unusual summer of 1994 in East Asia: IOD teleconnections. *Geophysical Research Letters*, 30(10), 1544. https://doi.org/10.1029/2002gl016831.

Ham, Y.-G., Kug, J.-S., Park, J.-Y. and Jin, F.-F. (2013) Sea surface temperature in the north tropical Atlantic as a trigger for El Nino/southern oscillation events. *Nature Geoscience*, 6(2), 112–116. http://www.nature.com/ngeo/journal/v6/n2/abs/ngeo1686.html#supplementary-information.

Harada, Y., Kamahori, H., Kobayashi, C., Endo, H., Kobayashi, S., Ota, Y., Onoda, H., Onogi, K., Miyaoka, K. and Takahashi, K. (2016) The JRA-55 reanalysis: representation of atmospheric circulation and climate variability. *Journal of the Meteorological Society of Japan Series II*, 94(3), 269–302. https://doi.org/10.2151/jmsj.2016-015.

Hong, X. and Lu, R. (2016) The meridional displacement of the summer Asian jet, silk road pattern, and tropical SST anomalies. *Journal of Climate*, 29(10), 3753–3766. https://doi.org/10.1175/JCLI-D-15-0541.1.

Hu, Z.-Z., Kumar, A., Xue, Y. and Jha, B. (2013) Why were some La Niñas followed by another La Niña? *Climate Dynamics*, 42, 1–14. https://doi.org/10.1007/s00382-013-1917-3.

Hu, K., Xie, S.-P. and Huang, G. (2017) Orographically anchored El Niño effect on summer rainfall in Central China. *Journal of Climate*, 30(24), 10037–10045. https://doi.org/10.1175/jcli-d-17-0312.1.

Huang, G. (2004) An index measuring the interannual variation of the east Asian summer monsoon—the EAP index. *Advances in Atmospheric Sciences*, 21(1), 41–52. https://doi.org/10.1007/bf02915679.

Huang, R. and Sun, F. (1992) Impacts of the tropical Western Pacific on the east Asian summer monsoon. *Journal of the Meteorological Society of Japan Series II*, 70(1B), 243–256. https://doi.org/10.2151/jmsj1965.70.1B_243.

Kao, H.Y. and Yu, J.Y. (2009) Contrasting eastern-Pacific and Central-Pacific types of ENSO. *Journal of Climate*, 22(3), 615–632.

Klein, S.A., Soden, B.J. and Lau, N.-C. (1999) Remote Sea surface temperature variations during ENSO: evidence for a tropical atmospheric bridge. *Journal of Climate*, 12(4), 917–932. https://doi.org/10.1175/1520-0442(1999)012<0917:rsstvd>2.0.co;2.

Kobayashi, S., Ota, Y., Harada, Y., Ebita, A., Moriya, M., Onoda, H., Onogi, K., Kamahori, H., Kobayashi, C., Endo, H., Miyaoka, K. and Takahashi, K. (2015) The JRA-55 reanalysis: general specifications and basic characteristics. *Journal of the Meteorological Society of Japan Ser II*, 93(1), 5–48. https://doi.org/10.2151/jmsj.2015-001.

Kosaka, Y. and Nakamura, H. (2010) Mechanisms of meridional teleconnection observed between a summer monsoon system and a subtropical anticyclone. Part I: the Pacific–Japan pattern. *Journal of Climate*, 23(19), 5085–5108. https://doi.org/10.1175/2010jcli3413.1.

Kosaka, Y. and Nakamura, H. (2011) Dominant mode of climate variability, intermodel diversity, and projected future changes over the summertime Western North Pacific simulated in the CMIP3 models. *Journal of Climate*, 24(15), 3935–3955. https://doi.org/10.1175/2011jcli3907.1.

Kosaka, Y., Nakamura, H., Watanabe, M. and Kimoto, M. (2009) Analysis on the dynamics of a wave-like teleconnection pattern along the summertime Asian jet based on a reanalysis dataset and climate model simulations. *Journal of the Meteorological Society of Japan Series II*, 87(3), 561–580. https://doi.org/10.2151/jmsj.87.561.

Kosaka, Y., Xie, S.P., Lau, N.C. and Vecchi, G.A. (2013) Origin of seasonal predictability for summer climate over the northwestern Pacific. *Proceedings of the National Academy of Sciences of the United States of America*, 110(19), 7574–7579. https://doi.org/10.1073/pnas.1215582110.

Kug, J.-S., Jin, F.-F. and An, S.-I. (2009) Two types of El Niño events: cold tongue El Niño and warm Pool El Niño. *Journal of Climate*, 22(6), 1499–1515. https://doi.org/10.1175/2008jcli2624.1.

Lau, K.-M. and Weng, H. (2001) Coherent modes of global SST and summer rainfall over China: An assessment of the regional impacts of the 1997–98 El Niño. *Journal of Climate*, 14(6), 1294–1308. https://doi.org/10.1175/1520-0442(2001)014<1294:cmogsa>2.0.co;2.

Lau, K.-M. and Wu, H.T. (2001) Principal modes of rainfall–SST variability of the Asian summer monsoon: a reassessment of the monsoon–ENSO relationship. *Journal of Climate*, 14(13), 2880–2895. https://doi.org/10.1175/1520-0442(2001)014<2880:pmorsv>2.0.co;2.

Lee, S.-K., DiNezio, P.N., Chung, E.-S., Yeh, S.-W., Wittenberg, A.T. and Wang, C. (2014) Spring persistence, transition, and resurgence of El Niño. *Geophysical Research Letters*, 41(23), 8578–8585. https://doi.org/10.1002/2014GL062484.

Li, G., Xie, S.-P. and Du, Y. (2015a) Climate model errors over the South Indian Ocean thermocline dome and their effect on the basin mode of interannual variability. *Journal of Climate*, 28, 3093–3098. https://doi.org/10.1175/jcli-d-14-00810.1.

Li, G., Xie, S.-P. and Du, Y. (2015b) Monsoon-induced biases of climate models over the tropical Indian Ocean. *Journal of Climate*, 28, 3058–3072. https://doi.org/10.1175/jcli-d-14-00740.1.

Li, G., Xie, S.-P., He, C. and Chen, Z. (2017) Western Pacific emergent constraint lowers projected increase in Indian summer monsoon rainfall. *Nature Climate Change*, 7, 708–712. https://doi.org/10.1038/nclimate3387, https://www.nature.com/articles/nclimate3387#supplementary-information.

Loon, H. and Rogers, J.C. (1978) The seesaw in winter temperatures between Greenland and northern Europe. Part I: general description. *Monthly Weather Review*, 106(3), 296–310. https://doi.org/10.1175/1520-0493(1978)106<0296:tsiwtb>2.0.co;2.

Lu, R.-Y., Oh, J.-H. and Kim, B.-J. (2002) A teleconnection pattern in upper-level meridional wind over the North African and Eurasian continent in summer. *Tellus A*, 54(1), 44–55. https://doi.org/10.1034/j.1600-0870.2002.00248.x.

Myers, N., Mittermeier, R.A., Mittermeier, C.G., da Fonseca, G.A.B. and Kent, J. (2000) Biodiversity hotspots for conservation priorities. *Nature*, 403(6772), 853–858. https://doi.org/10.1038/35002501.

Nie, Z.L., Gu, Z.J. and Sun, H. (2002) Cytological study of Tibetia (Fabaceae) in the Hengduan Mountains region, China. *Journal of Plant Research*, 115(1), 17–22. https://doi.org/10.1007/s102650200003.

Nitta, T. (1987) Convective activities in the tropical Western Pacific and their impact on the northern hemisphere summer circulation. *Journal of the Meteorological Society of Japan Series II*, 65(3), 373–390. https://doi.org/10.2151/jmsj1965.65.3_373.

North, G.R., Bell, T.L., Cahalan, R.F. and Moeng, F.J. (1982) Sampling errors in the estimation of empirical orthogonal functions. *Monthly Weather Review*, 110(7), 699–706. https://doi.org/10.1175/1520-0493(1982)110<0699:seiteo>2.0.co;2.

Ohba, M. and Ueda, H. (2007) An impact of SST anomalies in the Indian Ocean in acceleration of the El Niño to La Niña transition. *Journal of the Meteorological Society of Japan Series II*, 85(3), 335–348. https://doi.org/10.2151/jmsj.85.335.

Okumura, Y.M. and Deser, C. (2010) Asymmetry in the duration of El Niño and La Niña. *Journal of Climate*, 23(21), 5826–5843. https://doi.org/10.1175/2010jcli3592.1.

Qiu, Y., Cai, W.J., Guo, X.G. and Ng, B. (2014) The asymmetric influence of the positive and negative IOD events on China's rainfall. *Scientific Reports*, 4, 4943. https://doi.org/10.1038/srep04943.

Saji, N.H. and Yamagata, T. (2003) Possible impacts of Indian Ocean dipole mode events on global climate. *Climate Research*, 25(2), 151–169.

Schneider, U., Becker, A., Finger, P., Meyer-Christoffer, A., Ziese, M. and Rudolf, B. (2014) GPCC's new land surface precipitation climatology based on quality-controlled in situ data and its role in quantifying the global water cycle. *Theoretical and Applied Climatology*, 115(1), 15–40. https://doi.org/10.1007/s00704-013-0860-x.

Simmonds, I., Bi, D. and Hope, P. (1999) Atmospheric water vapor flux and its association with rainfall over China in summer. *Journal of Climate*, 12(5), 1353–1367. https://doi.org/10.1175/1520-0442(1999)012<1353:awvfai>2.0.co;2.

Smith, T.M. and Reynolds, R.W. (2003) Extended reconstruction of global sea surface temperatures based on COADS data (1854–1997). *Journal of Climate*, 16(10), 1495–1510. https://doi.org/10.1175/1520-0442-16.10.1495.

Song, J., Li, C. and Zhou, W. (2014) High and low latitude types of the downstream influences of the North Atlantic oscillation. *Climate Dynamics*, 42(3–4), 1097–1111. https://doi.org/10.1007/s00382-013-1844-3.

Su, J., Zhang, R., Li, T., Rong, X., Kug, J.S. and Hong, C.-C. (2010) Causes of the El Niño and La Niña amplitude asymmetry in the equatorial eastern Pacific. *Journal of Climate*, 23(3), 605–617. https://doi.org/10.1175/2009jcli2894.1.

Sun, J. and Wang, H. (2012) Changes of the connection between the summer North Atlantic oscillation and the east Asian summer rainfall. *Journal of Geophysical Research: Atmospheres*, 117(D8), D08110. https://doi.org/10.1029/2012jd017482.

Takahashi, K. and Dewitte, B. (2016) Strong and moderate nonlinear El Niño regimes. *Climate Dynamics*, 46(5), 1627–1645. https://doi.org/10.1007/s00382-015-2665-3.

Tan, L., Cai, Y., Cheng, H., Edwards, L.R., Lan, J., Zhang, H., Li, D., Ma, L., Zhao, P. and Gao, Y. (2018) High resolution monsoon precipitation changes on southeastern Tibetan plateau over the past 2300 years. *Quaternary Science Reviews*, 195, 122–132. https://doi.org/10.1016/j.quascirev.2018.07.021.

Tao, W., Huang, G., Hu, K., Qu, X., Wen, G. and Gong, Y. (2014) Different influences of two types of El Niños on the Indian Ocean SST variations. *Theoretical and Applied Climatology*, 117 (3–4), 475–484. https://doi.org/10.1007/s00704-013-1022-x.

Tao, W., Huang, G., Hu, K., Gong, H., Wen, G. and Liu, L. (2016) A study of biases in simulation of the Indian Ocean basin mode and its capacitor effect in CMIP3/CMIP5 models. *Climate Dynamics*, 46(1), 205–226. https://doi.org/10.1007/s00382-015-2579-0.

Tao, W., Huang, G., Wu, R., Hu, K., Wang, P. and Chen, D. (2017) Asymmetry in summertime atmospheric circulation anomalies over the Northwest Pacific during decaying phase of El Niño and La Niña. *Climate Dynamics*, 49(5), 2007–2023. https://doi.org/10.1007/s00382-016-3432-9.

Tao, W., Huang, G., Wu, R., Hu, K., Wang, P. and Gong, H. (2018) Origins of biases in CMIP5 models simulating Northwest Pacific summertime atmospheric circulation anomalies during the decaying phase of ENSO. *Journal of Climate*, 31(14), 5707–5729. https://doi.org/10.1175/jcli-d-17-0289.1.

Tao, W., Huang, G., Wang, P., Liu, Y., Wen, G. and Dong, D. (2019) Dominant modes of CMIP3/5 models simulating Northwest Pacific circulation anomalies during post-ENSO summer and their SST dependence. *Theoretical and Applied Climatology*, 138 (3), 1809–1820. https://doi.org/10.1007/s00704-019-02936-3.

Tao, W., Huang, G., Lau, W.K.M., Dong, D., Wang, P. and Wen, G. (2020) How can CMIP5 AGCMs' resolution influence precipitation in mountain areas: the Hengduan Mountains? *Climate Dynamics*, 54(1), 159–172. https://doi.org/10.1007/s00382-019-04993-w.

Trenberth, K.E. and Stepaniak, D.P. (2001) Indices of El Nino evolution. *Journal of Climate*, 14(8), 1697–1701. https://doi.org/10.1175/1520-0442(2001)014<1697:lioeno>2.0.co;2.

Walker, G.T. (1924) Correlation in seasonal variations of weather, IX. A further study of world weather. *Memoirs of the India Meteorological Department*, 24(9), 275–333.

Wallace, J.M. and Gutzler, D.S. (1981) Teleconnections in the geopotential height field during the northern hemisphere winter. *Monthly Weather Review*, 109(4), 784–812. https://doi.org/10.1175/1520-0493(1981)109<0784:titghf>2.0.co;2.

Wang, B., Wu, R.G. and Fu, X.H. (2000) Pacific-east Asian teleconnection: how does ENSO affect east Asian climate? *Journal of Climate*, 13(9), 1517–1536. https://doi.org/10.1175/1520-0442(2000)013<1517:peathd>2.0.co;2.

Wang, B., Wu, R. and Lau, K.M. (2001) Interannual variability of the Asian summer monsoon: contrasts between the Indian and the Western North Pacific–east Asian monsoons. *Journal of Climate*, 14(20), 4073–4090. https://doi.org/10.1175/1520-0442(2001)014<4073:ivotas>2.0.co;2.

Wang, B., Xiang, B. and Lee, J.-Y. (2013) Subtropical high predictability establishes a promising way for monsoon and tropical storm predictions. *Proceedings of the National Academy of Sciences*, 110(8), 2718–2722. https://doi.org/10.1073/pnas.1214626110.

Wang, Z., Yang, S., Lau, N.-C. and Duan, A. (2018) Teleconnection between summer NAO and East China rainfall variations: a bridge effect of the Tibetan plateau. *Journal of Climate*, 31(16), 6433–6444. https://doi.org/10.1175/jcli-d-17-0413.1.

Wang, B., Luo, X., Yang, Y.-M., Sun, W., Cane, M.A., Cai, W., Yeh, S.-W. and Liu, J. (2019) Historical change of El Niño properties sheds light on future changes of extreme El Niño. *Proceedings of the National Academy of Sciences*, 116(45), 22512. https://doi.org/10.1073/pnas.1911130116.

Wei, W., Zhang, R., Wen, M., Rong, X. and Li, T. (2014) Impact of Indian summer monsoon on the south Asian high and its influence on summer rainfall over China. *Climate Dynamics*, 43(5), 1257–1269. https://doi.org/10.1007/s00382-013-1938-y.

Wu, R. (2002) A mid-latitude Asian circulation anomaly pattern in boreal summer and its connection with the Indian and east Asian summer monsoons. *International Journal of Climatology*, 22(15), 1879–1895. https://doi.org/10.1002/joc.845.

Wu, L. and Liu, Z. (2002) Is tropical Atlantic variability driven by the North Atlantic oscillation. *Geophysical Research Letters*, 29 (13), 31-31–31-34. https://doi.org/10.1029/2002gl014939.

Wu, Z., Wang, B., Li, J. and Jin, F.-F. (2009) An empirical seasonal prediction model of the east Asian summer monsoon using ENSO and NAO. *Journal of Geophysical Research: Atmospheres*, 114(D18), D18120. https://doi.org/10.1029/2009jd011733.

Wu, B., Li, T. and Zhou, T. (2010) Relative contributions of the Indian Ocean and local SST anomalies to the maintenance of the Western North Pacific anomalous anticyclone during the El Niño decaying summer*. *Journal of Climate*, 23(11), 2974–2986. https://doi.org/10.1175/2010jcli3300.1.

Wu, R., Yang, S., Liu, S., Sun, L., Lian, Y. and Gao, Z. (2011) Northeast China summer temperature and North Atlantic SST. *Journal of Geophysical Research: Atmospheres*, 116(D16), D16116. https://doi.org/10.1029/2011jd015779.

Wu, B., Zhou, T. and Li, T. (2017) Atmospheric dynamic and thermodynamic processes driving the Western North Pacific anomalous anticyclone during El Niño. Part I: maintenance mechanisms. *Journal of Climate*, 30(23), 9621–9635. https://doi.org/10.1175/jcli-d-16-0489.1.

Xie, S.P. and Carton, J.A. (2004) Tropical Atlantic variability: patterns, mechanisms, and impacts. In: Wang, C., Xie, S.P. and Carton, J.A. (Eds.) *Earth's Climate: The Ocean-Atmosphere Interaction*, Vol. 147. Geophysical Monograph Book Series. Washington: Amer Geophysical Union, pp. 121–142.

Xie, S.P., Annamalai, H., Schott, F.A. and McCreary, J.P., Jr. (2002) Structure and mechanisms of south Indian Ocean climate variability. *Journal of Climate*, 15(8), 864–878.

Xie, S.P., Hu, K., Hafner, J., Tokinaga, H., Du, Y., Huang, G. and Sampe, T. (2009) Indian Ocean capacitor effect on indo-western Pacific climate during the summer following El Niño. *Journal of Climate*, 22(3), 730–747.

Xing, Y. and Ree, R.H. (2017) Uplift-driven diversification in the Hengduan Mountains, a temperate biodiversity hotspot. *Proceedings of the National Academy of Sciences*, 114(17), E3444–E3451. https://doi.org/10.1073/pnas.1616063114.

Yang, Y., Wu, R. and Wang, C. (2020) Individual and combined impacts of tropical Indo-Pacific SST anomalies on interannual variation of the Indochina peninsular precipitation. *Journal of Climate*, 33(3), 1069–1088. https://doi.org/10.1175/jcli-d-19-0262.1.

Yasui, S. and Watanabe, M. (2010) Forcing processes of the summertime circumglobal teleconnection pattern in a dry AGCM. *Journal of Climate*, 23(8), 2093–2114. https://doi.org/10.1175/2009jcli3323.1.

Yeh, S.W., Kug, J.S., Dewitte, B., Kwon, M.H., Kirtman, B.P. and Jin, F.F. (2009) El Nino in a changing climate. *Nature*, 462 (7273), 511–514. https://doi.org/10.1038/nature08546.

Yuan, Y., Yang, H., Zhou, W. and Li, C. (2008) Influences of the Indian Ocean dipole on the Asian summer monsoon in the following year. *International Journal of Climatology*, 28(14), 1849–1859. https://doi.org/10.1002/joc.1678.

Zhang, P., Li, G., Fu, X., Liu, Y. and Li, L. (2014) Clustering of Tibetan plateau vortices by 10–30-day intraseasonal oscillation. *Monthly Weather Review*, 142(1), 290–300. https://doi.org/10.1175/mwr-d-13-00137.1.

Zhang, T., Li, B., He, Y., Du, J., Niu, H. and Xin, H. (2015) Spatial and temporal distribution of precipitation based on corrected TRMM data in Hengduan Mountains (in Chinese). *Journal of Natural Resources*, 30(2), 260–270.

Zhao, G., Huang, G., Wu, R., Tao, W., Gong, H., Qu, X. and Hu, K. (2015) A new upper-level circulation index for the east Asian summer monsoon variability. *Journal of Climate*, 28(24), 9977–9996. https://doi.org/10.1175/JCLI-D-15-0272.1.

Zhou, C., Jiang, X., Li, Y. and Wei, G. (2009) Features of climate change of water vapor resource over eastern region of the Tibetan plateau and its surroundings (in Chinese). *Plateau Meteorology*, 28(1), 55–63.

Zhu, G., Pu, T., Zhang, T., Liu, H., Zhang, X. and Liang, F. (2013) The accuracy of TRMM precipitation data in Hengduan mountainous region, China (in Chinese). *Scientia Geographica Sinica*, 33(9), 1125–1131. https://doi.org/10.13249/j.cnki.sgs.

Zhu, G., Qin, D., Tong, H., Liu, Y., Li, J., Chen, D., Wang, K. and Hu, P. (2016) Variation of Thornthwaite moisture index in Hengduan Mountains, China. *Chinese Geographical Science*, 26 (5), 687–702. https://doi.org/10.1007/s11769-016-0820-3.

SUPPORTING INFORMATION

Additional supporting information may be found online in the Supporting Information section at the end of this article.

How to cite this article: Tao W, Huang G, Dong D, Wang P, Yu T, Gong H. Dominant modes of interannual variability in precipitation over the Hengduan Mountains during rainy seasons. *Int J Climatol*. 2021;41:2795–2809. https://doi.org/10.1002/joc.6990